Control Engineering Practice 18 (2010) 1084–1092

Contents lists available at ScienceDirect

Control Engineering Practice

journal homepage: www.elsevier.com/locate/conengprac

Co-operative path planning of multiple UAVs using Dubins paths with clothoid arcs

Madhavan Shanmugavel, Antonios Tsourdos *, Brian White, Rafał Żbikowski

Department of Informatics and Sensors, Cranfield Defence and Security, Defence Academy of the UK, Shrivenham, Swindon SN6 8LA, UK

ARTICLE INFO

Article history:
Received 6 February 2008
Accepted 18 February 2009
Available online 3 April 2009

Keywords:
Path planning
Dubins paths
Clothoid paths
UAV
Co-operative trajectories

ABSTRACT

This paper describes co-operative path planning of a group of unmanned aerial vehicles (UAVs). The problem undertaken for this study is that of simultaneous arrival on target of a group of UAVs. The problem of path planning is formulated in order to produce feasible (flyable and safe) paths and the solution is divided into three phases. The first phase is that of producing flyable paths, the second is to add extra constraints to produce safe paths that do not collide with other UAV members or with known obstacles in the environment, and the third is to produce paths for simultaneous arrival. In the first phase, Dubins paths with clothoid arcs are used to produce paths for each UAV. These paths are produced using the principles of differential geometry. The second phase manipulate these paths to make them safer by meeting safety constraints: (i) to maintain minimum separation distance, (ii) to produce non-intersection of paths at equal lengths, and (iii) to fly-through intermediate way-points/poses. Finally, in the third phase, the simultaneous arrival is achieved by making all the paths equal in lengths. Some simulation results are given to illustrate the technique.

1. Introduction

Autonomy is replacing the human operator in many applications. Examples are military systems where there is some element of danger to the human operator, handling hazardous materials, disaster managements, and in monotonous operations such as surveillance and reconnaissance. The replacement of the human operator in such systems necessitates the development of autonomous systems techniques. Such autonomous systems operates in many environments such as air, water, space or on land. However, in this study, unmanned aerial vehicles (UAVs) are studied, operating as a group. The large range of potential applications of UAVs in military and in civilian sectors have generated a lot academic as well as commercial research (Wilson, 2007). The rapid development of low-cost electronics makes the deployment of UAVs more practical. Inspired by examples in nature such as flocks of birds and schools of fish, one of the active researches in autonomous systems is co-operative control (Rabbath, Gagnon, & Lauzon, 2004; Uny Cao, Fukunaga, & Kahng, 1997). Employing a group of UAVs rather than a single UAV can result in cost-effective and fault tolerant systems.

One function of the UAV is to be a mobile sensor platform which is required to fly from one location to another whilst performing surveillance or tracking. This requires the planning of suitable safe paths for the UAVs which is provided by a path-planner. The path-planner is a sub-system of a mission planner and a typical and functional architecture of the mission planner is shown in Fig. 1. The figure shows three sub-systems or layers, however, the number of sub-systems and their functions may vary for different applications and objectives of the mission. The first layer holds and keeps track of objective of the mission. Based on these objectives, this layer allocates resources and tasks to the UAVs and also acts as decision-maker. The intermediate (second) layer produces paths/trajectories for the UAVs. In this layer, the path planning and their associated algorithms such as collision avoidance to produce feasible trajectories/paths are located. The lower (third) level produces guidance and control actions which ensure the UAVs fly on the reference trajectories produced at the second level. This paper focuses on layer 2, where the path-planner produces trajectories to fulfil the mission objectives. The mission objective considered here is the simultaneous arrival at a specified location by a group of UAVs.

Path planning is still one of the open problems in the field of autonomous systems. The path-planner generates one or more paths between two or more points. Normally, the points are specified locations on a stored map. Path planning is a complex problem, which involves meeting physical constraints of the UAVs, constraints from operating environment and other operational requirements. The foremost constraint to be met is that the paths must be flyable. Flyable paths are those that meet the kinematic constraints of the UAV. Satisfying this constraint ensures that the motion of the UAVs stays within the maximum bounds on

* Corresponding author.
E-mail address: a.tsourdos@cranfield.ac.uk (A. Tsourdos).

0967-0661/$ - see front matter © 2009 Elsevier Ltd. All rights reserved.
doi:10.1016/j.conengprac.2009.02.010

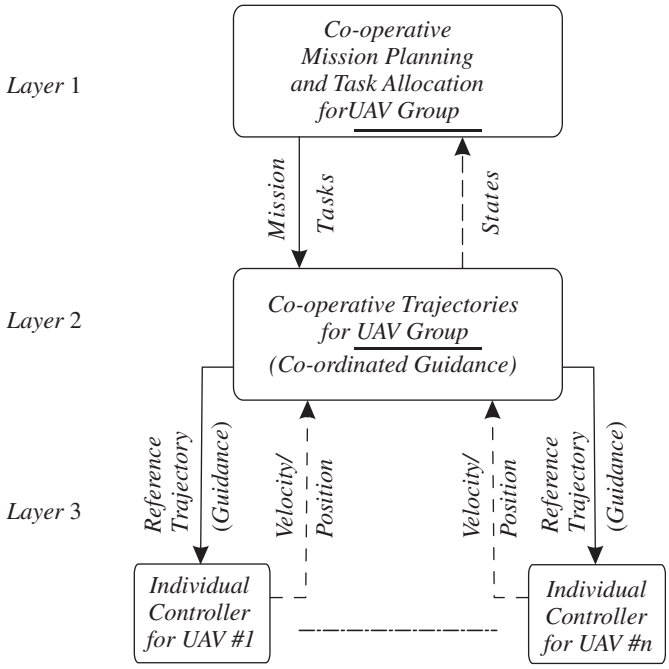

Fig. 1. Hierarchy of mission planning.

manoeuvre curvature. The curvature is proportional to the UAV lateral acceleration ($\vec{a} = \kappa \vec{v}^2$), where $\vec{a}$ is the lateral acceleration, κ the curvature, and $\vec{v}$ the velocity. Curvature at all points on the path must be less than the maximum curvature of the UAVs. Hence, the path curvature determines whether a path is flyable or not (in 3D, it is determined by both the curvature and torsion) (Lipschutz, 1969).

The second important constraint is safety. The safety of the path is measured by ability of the path to avoid threats, obstacles, and other UAVs. The path must maintain collision avoidance with other friendly UAVs and also must be flexible enough to avoid the environmental obstacles and threats. Also, additional constraints such as generating shortest paths, minimum fuel and energy consumption paths can be included for better performance and efficiency of the mission. The shortest path solution is considered in this paper as it is also usually close to the most energy efficient path. There may be other constraints such as maintaining communication in a complex urban environment, as well as time, task completion, and resource management depending on the mission objectives. Hence, producing flyable and safe (labelled feasible) paths of equal lengths in the presence of static obstacles in the environment for a group of UAVs for simultaneous arrival on target is the subject of this paper.

2. Prior work

Path planning for multiple UAVs is an active research area in recent times. The objectives and approaches differ depending on the application domain: surveillance, search and track, rescue missions, and disaster monitoring. Currently, there are a multitude of solution approaches available in the research literature and each approach has its own merits. Moreover, new approaches are required as the complexity of the problem increases. However, the majority of solution-approaches can be represented by a simplified diagram as shown in Fig. 2. Using this approach, the inputs to the path-planner are the way-points, the obstacle positions and size, and the associated uncertainties. Optimization techniques are applied to this data to produce routes. The

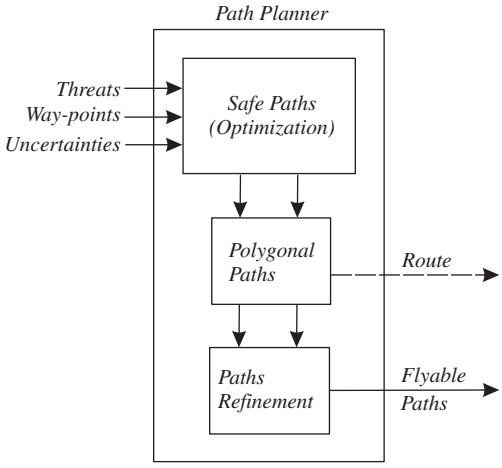

Fig. 2. Existing approach to path planning.

resulting routes are usually polygonal paths which do not have inherent curvature constraints built into the solution. In some cases the path-planner ends with the generation of the routes and in other cases, these routes are further refined to produce flyable paths by elimination of un-flyable paths.

In the literature, a wide variety of approaches are used to produce routes from input data. In the Voronoi diagram approach (Chandler, Rasmussen, & Pachter, 2000), the routes are generated for a given map which defines the set of static obstacles. In operation, the Voronoi diagram is updated for every pop-up threat encountered. In Mclain and Beard (2000), the analogy of a chain connecting the end-points is considered to produce feasible paths by defining chain link forces to reduce direction changes. The safe paths are produced by defining a repulsive forces associated with the obstacles. These forces restrict the path to large changes in shape and close approach to obstacles. A similar approach is studied by defining virtual forces in Bortoff (2000). Trajectory smoothing applied to cubic splines to produce routes and is presented in Judd and McClain (2001) and applied to arcs in Chandler, Pachter, and Rasmussen (2001). Straight line trajectories are assumed in task allocation for multiple robots problems in Zhang, Wang, and Yu (2008) and Shima, Rasmussen, and Sparks (2005). Optimization techniques such as mixed integer linear programming (Schouwenaars, Feron, & How, 2006), evolutionary algorithms (Dong & Vagners, 2004; Nikolos, Valavanis, Tsourveloudis, & Kostaras, 2003; Zheng, Li, Xu, Sun, & Ding, 2005) have also been used for the path planning of UAVs.

A comprehensive review of types of paths used for path planning is presented in Segovia, Rombaut, Preciado, and Meizel (1991). Also, there are researches, who consider the path planning as an integral part. A rendezvous application which generates coordinated trajectory is dealt in Chandler et al. (2000). An optimal path generation to avoid radar exposure is studied using analytical and discrete optimization approaches with the constraint on the path length in Zabarankin, Uryasev, and Pardalos (2001). The path planning problem is treated as a search problem in the partitioned cells in Eagle and Yee (1990). A comparative study of path planning using graph, optimal control, and potential field methods to avoid enemy radar sites can be seen in Bortoff (2000). Parametric curves are used for path planning in Shanmugavel, Tsourdos, Żbikowski, White, Rabbath, and Lechevin (2006) and Nikolos et al. (2003). Dubins path for path planning of UAVs can be found in Shanmugavel, Tsourdos, Żbikowski, and White (2006) and Shanmugavel, Tsourdos, Żbikowski, and White (2005).

This paper describes a new approach to path planning, which is illustrated in Fig. 3. This approach uses flyable paths for path

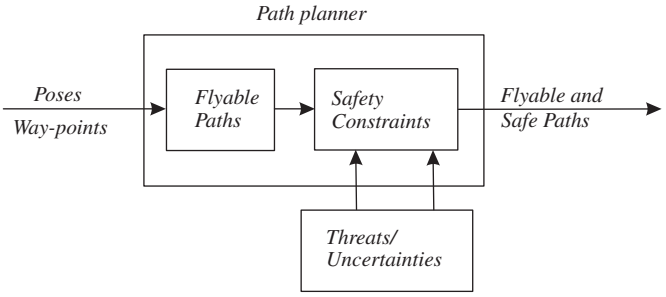

Fig. 3. New approach to path planning.

planning. The flyable paths are first produced separately to connect the way-points and their associated poses. The resulting flyable paths are kinematically feasible paths which satisfy the motion constraints of the UAVs. These paths are then adjusted to produce safe paths, which meet additional safety constraints. The flyable paths are based on Dubins path (Dubins, 1957) but with the circular arcs replaced with clothoid arcs, and are designed using the principle of differential geometry. Earlier use of the clothoid curve can be seen in robotic applications (Scheuer & Fraichard, 1997). However, by the best of the author's knowledge, this is the first paper providing a design of Dubins path with clothoid arcs using the principles of differential geometry. The main contribution of this paper is the design of a flight path using the principles of differential geometry and the using them for path planning of multiple UAVs.

The paper is organized as follows: Section 3 describes the mission, its objectives and the assumptions. Formulation of path planning problem is then described in Section 4. The following Section 5 details the solution approach and its phases. In Section 7, the mathematical derivation of flyable path is described. The simulations and results in free environment and cluttered space are discussed in Section 8. Finally, the paper ends with discussions and conclusions.

3. Scenario

Fig. 4 shows the schematic for the problem. A group of N UAVs leaving from a base and they have to reach the target area at the same time. The individual start and finish points for each UAV are represented by position coordinates (x,y,z) and orientation by angle (θ,ϕ) and are assumed to be known a priori. The UAVs are assumed to be of same type and are flying at same the speed at constant altitude. Each UAV has the same maximum bound on its curvature and the environment has static obstacles. The UAVs are required to avoid collision with other UAVs and with other objects in the air-space, as well as avoiding the static obstacles.

4. Problem formulation

Consider initially the path planning of a single UAV from the base to the target position with no constraints. The starting point P_s is at the base position and the finishing point P_f is at the target position. The path connecting the poses is represented by the label r. The path-planner produces a path connecting the start pose $p_s(x_s,y_s,z_s,\theta_s,\phi_s)$ and the finish pose $p_f(x_f,y_f,z_f,\theta_f,\phi_f)$.

$$P_s(x_s,y_s,z_s,\theta_s,\phi_s) \xrightarrow{r(t)} P_f(x_f,y_f,z_f,\theta_f,\phi_f) \tag{1}$$

where t is a path-length parameter.

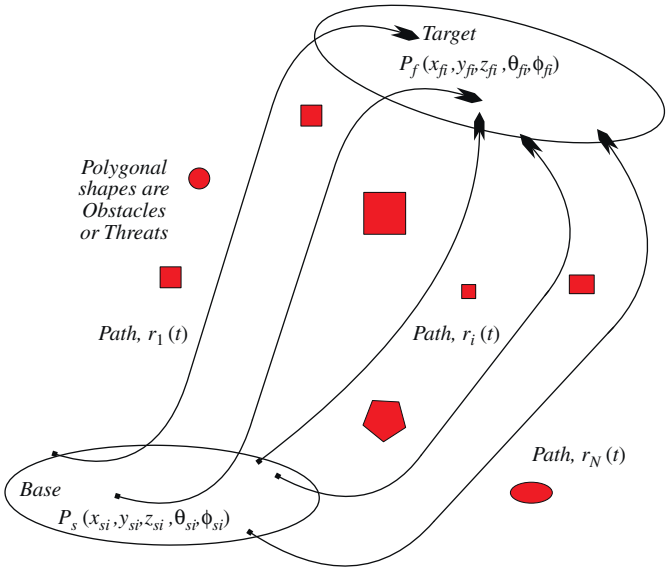

Fig. 4. Scenario: $r_i(t)$—flight paths, (x,y,z)—position coordinates, (θ,ϕ)—orientations, and the boxes in red—obstacles. Suffix i represents ith UAV or path. (For interpretation of the references to the colour in this figure legend, the reader is referred to the web version of this article.)

Extending Eq. (1) to account for N UAVs such that each UAV passes through n_p number of positions poses, gives

$$\begin{aligned} &P_{s,i,j-1}(x_{s,i,j-1},y_{s,i,j-1},z_{s,i,j-1},\theta_{s,i,j-1},\phi_{s,i,j-1}) \\ &\quad \xrightarrow{r_{i,j-1}(t)} P_{f,i,j}(x_{f,i,j},y_{f,i,j},z_{f,i,j},\theta_{f,i,j},\phi_{f,i,j}), \\ &|\kappa(t)|<\kappa_{max},\,|\tau(t)|<\tau_{max},\,\coprod_{safe},\,\coprod_{length}, \\ &\qquad i=1\ldots N,\;\; j=2\ldots n_p,\;\; n_p\geqslant 2 \end{aligned} \tag{2}$$

where τ is the path torsion, κ the path curvature, κ_{max} the maximum curvature bound, τ_{max} the maximum bound on torsion, and $\coprod_{safe}$ and $\coprod_{length}$ are the constraints on safety and path length, respectively.

The safety constraints are described in Sections 5.2.1–5.2.3. The constraint on length is

$$\coprod_{length} = \min \int_{s_1}^{s_2} s(t) \tag{3}$$

$$\text{where } s(t) = \int_{t_1}^{t_2} \sqrt{\dot{x}(t)^2+\dot{y}(t)^2+\dot{z}(t)^2}\,dt,\;\; t\in[t_1,t_2] \tag{4}$$

For flights at constant altitude, the Eq. (2) reduces to

$$\begin{aligned} &P_{s,i,j-1}(x_{s,i,j-1},y_{s,i,j-1},\theta_{s,i,j-1}) \xrightarrow{r_{i,j-1}(t)} P_{f,i,j}(x_{f,i,j},y_{f,i,j},\theta_{f,i,j}), \\ &|\kappa_i(t)|<\kappa_{max},\,\coprod_{safe},\,\coprod_{length},\quad i=1\ldots N,\;\; j=2\ldots n_p,\;\; n_p\geqslant 2 \end{aligned} \tag{5}$$

Eq. (1) is solved using a Dubins approach for the 2D case with curvature constraints (Dubins, 1957). This showed that the shortest path is made of either three tangential circular arcs (CCC type) or two circular arcs tangential with the straight line in the middle (CLC type) or a subset of the two, where 'C' represents circular manoeuvre, and 'L' represents straight line manoeuvre.

5. Solution description

For UAVs all flying at constant equal speeds, simultaneous arrival can be achieved by producing paths of equal lengths. This can be achieved by solving the Eq. (5) with an extra constraint on

paths: $s_k(t) = s_m(t)$ such that length of kth and mth paths are equal. As adding constraints increase complexity and may not result in an optimal solution, the problem is broken down into three phases. In the first phase, the shortest flyable paths are produced for each UAV. The second phase solves the safety constraints and in the third phase flight paths of equal lengths are produced.

5.1. Phase I: selection of flyable path

In the first phase, flyable paths connect the start to finish poses of each UAV. The flyable path is defined to be the shortest and have continuous curvature which satisfies the maximum curvature constraints of the UAVs. In the first instance, Dubins path with clothoid arcs are chosen, where the straight line tangentially joined to two circular arcs (*circle–line–circle*). The curvature profile of this path has two discontinuities. Hence, the circular arcs are replaced with clothoid arcs which have ramp curvature profile. This modification provides a smooth curvature transition between the arcs and the line segment. The paths and their curvature profiles are shown in Fig. 5.

The curvature of the path is proportional to lateral acceleration, which, together with other states, velocity, and position, form a closed-loop guidance system that provides path tracking (third layer in Fig. 1). The path-planning and path-tracking together form a closed-loop feedback, which ensured that the UAVs can accurately follow the designated paths.

5.2. Phase II: meeting safety constraints

In the second phase, the flyable paths are tuned to meet the safety constraints. These constraints take into account the known obstacles and collision avoidance amongst the UAV group. Each UAV is assumed to have a safety disc of radius R, located at the UAV centre of mass. The value of this radius is less than the sensor range but greater than the minimum radius of curvature. This ensures that the UAV can sense an obstacle or other UAV and have sufficient manoeuvre capability to avoid collision.

Two constraints: (i) minimum separation distance and (ii) non-intersection at equal path lengths are shown in Fig. 6. The third

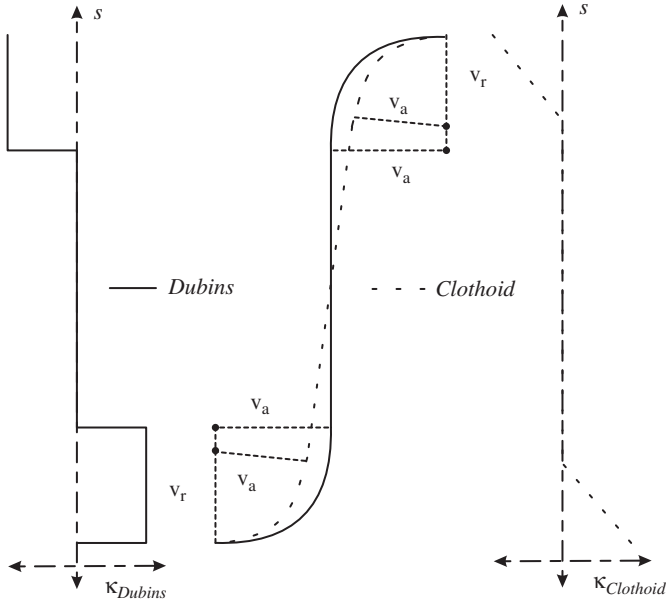

Fig. 5. Flyable paths and their curvature profiles.

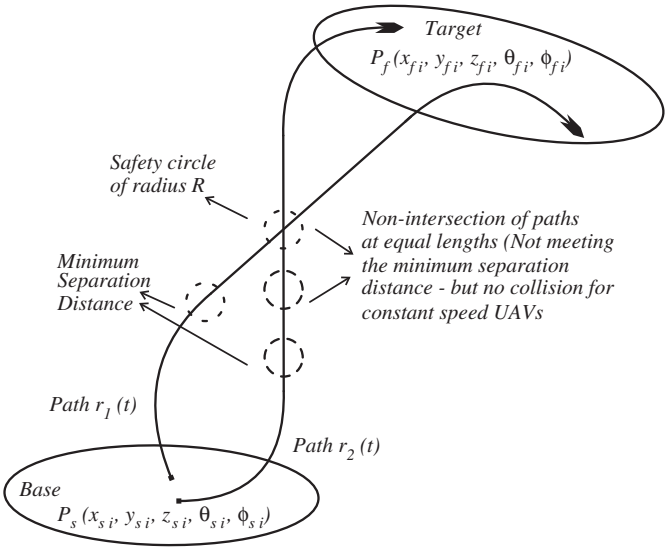

Fig. 6. Safe flight path.

safety constraint which handles the pop-up obstacles by producing intermediate way-point/pose, discussed in Section 5.2.3.

5.2.1. Minimum separation distance

The distance between any two flight paths should be less than a threshold value, called minimum separation distance. Here it is taken as two times the radius of the safety circle. Refer to Fig. 6. If the safety circles of any two paths overlap, a collision occurs. The paths are re-planned either to pass through new way-point/pose or the trace/shape of the path is changed by varying the curvature of the arcs. Representing the distance between $r_k(t)$ and $r_m(t)$ paths by $d_{k,m}$, the constraint of minimum separation distance is

$$d_{sep} = d_{k,m} > 2R_s \tag{6}$$

5.2.2. Non-intersection of paths at equal length

The previous constraint holds good for UAVs flying in straight lines, but not for curved paths. For curved path, the 'minimum separation distance' may give a false result. Referring to the Fig. 6, the paths: $r_k(t)$ and $r_m(t)$ intersect at a point X. Hence, they fail to meet the minimum separation distance. However, this may be a false result, if the distance travelled by each UAV from their starting points to the intersection point are not equal. Hence collision is avoided if the difference between the lengths of the paths to the intersection point is greater than the safety circle value.

$$d_{int} = |d_{k,int} - d_{m,int}| > 2R_s \tag{7}$$

where $d_{k,int}$ and $d_{m,int}$ are the lengths of the paths $r_k(t)$ and $r_m(t)$, respectively, from their starting points to the intersection point.

The flyable paths are tested for satisfaction of the safety constraints. If the paths meet the safety constraints in Eqs. (6) and (7), there is no need for re-planning the paths. Otherwise, the paths are re-planned by varying the curvature of the clothoid arcs or by flying through intermediate way-points.

5.2.3. Handling threats using intermediate way-point/pose

Although the above two constraints provide collision avoidance, handling static obstacles is best handled by generating intermediate way-points/poses. When the path intersects with the obstacle, the path-planner generates an intermediate way-point so that the obstacle is avoided. Consider a flyable trajectory $r(t)$ generated for a given set of poses/waypoints. The threat

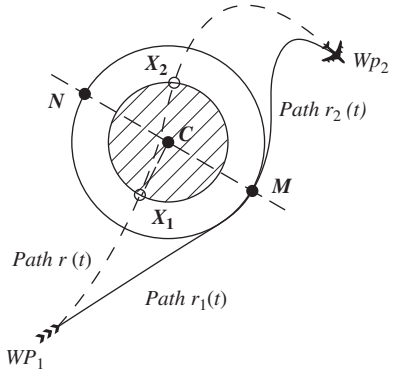

Fig. 7. Threat handling by intermediate pose.

avoidance algorithm calls the path-planner to re-plan the nominal path obtained prior to occurrence of an obstacle, by selecting a new way-point/pose. The schematic of the concept is given in Fig. 7. In the figure, the central hatched circle is an obstacle. The intermediate way-point M is selected based on the location of the centre of the obstacle C, which is either to the left or the right of the line connecting the intersection points X_1 and X_2. If the centre C is left to the line X_1–X_2, the intermediate pose M is selected on right to the obstacle region and vice versa. Points M and N on the safety circle are the intermediate poses. These points are generated by intersection of the normal to the line segment X_1–X_2 with the safety circle. In the figure, the initial path is $r(t)$ and the new paths generated with the intermediate way-point M are $r1(t)$ and $r2(t)$ and wp_1 and wp_2 are the way-points/poses.

6. Phase III: paths of equal length

The mission objective is simultaneous arrival on target. This requires that the length of all the UAV paths should be equal. However, the feasible (flyable and safe) paths produced by meeting the curvature and safety constraints are not equal in length. Hence the length of the feasible paths are adjusted to equal to that of a reference path. The longest of the group of UAV paths is taken as the reference path and the length of the other paths are increased to that of the reference path.

Path length is the cumulative sum of length of clothoid arcs and the tangent line connecting the arcs. The length of the paths are increased by decreasing the curvature of the clothoid arcs iteratively and vica versa.

$$s_{ref} = \max(\{s_i\}), \quad i = 1, \ldots, N \tag{8}$$

The value of curvature κ is calculated by solving

$$s_{ref} - \{s_i\} = 0, \quad i = 1, \ldots, N-1 \tag{9}$$

where s is the length of the path, $\{s\}$ the set of path lengths, N the number of UAVs, and s_{ref} the length of the reference path.

7. Design of flyable path

7.1. Frenet–Serret frame

The flyable path is designed using the principles of linear algebra and differential geometry. By differential geometry, a curve in 2D is generated by a moving ortho-normal frame. Each point on the curve has a tangent and a normal vectors together form a sequence of ortho-normal frames. These frames are called Frenet–Serret frames (Lipschutz, 1969). Consider the point Q on the curve $r(t)$ in Fig. 8. The unit tangent and normal vectors at Q are represented as T and N, respectively. The tangent T makes an angle of θ with x-axis and the length of the path at Q is s. The evolution of frame with increasing path length and equations of frame at Q are given by

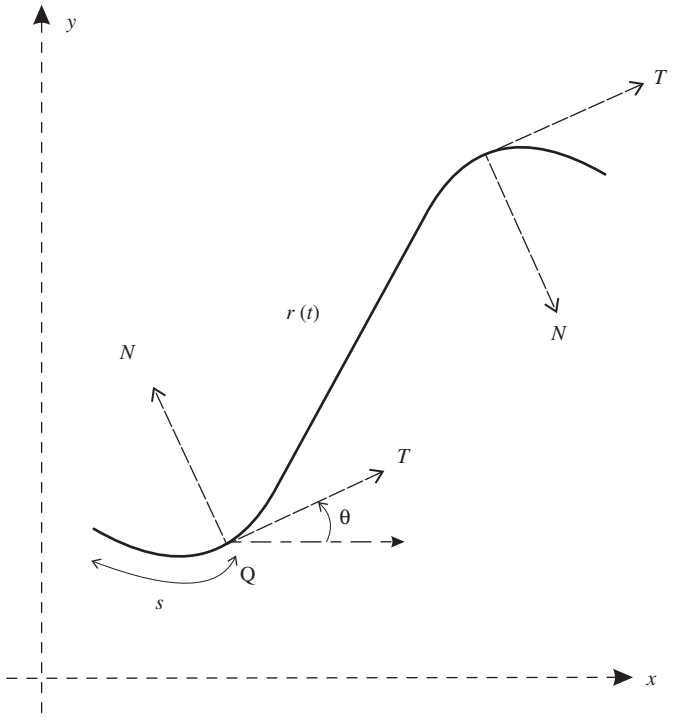

Fig. 8. Frenet–Serret frame in 2D.

$$T' = \kappa(s)N = \frac{dT}{ds} \tag{10}$$

$$N' = -\kappa(s)T = \frac{dN}{ds} \tag{11}$$

$$T = \frac{dx}{ds} = \cos(\theta) \tag{12}$$

$$N = \frac{dy}{ds} = \sin(\theta) \tag{13}$$

$$\kappa = \frac{d\theta}{ds} \tag{14}$$

7.2. Clothoid arcs

For a clothoid arc, the arc angle varying along the trajectory is given by

$$\theta(t) = \int_0^t \kappa \frac{\tau}{s}\, d\tau = \frac{\kappa}{2s} t^2 \tag{15}$$

where κ is the curvature at arc length s and t the arc length variable, such that $s = |\vec{v}|t$, where $\vec{v}$ is the velocity. The position vector of the end point is given by the x and y positions. These are obtained by integration:

$$x(s) = \int_0^s \cos(\theta)\, dt$$

$$y(s) = \int_0^s \sin(\theta)\, dt \tag{16}$$

The angle θ_t through which the trajectory moves over the total arc length s is $\theta_t = \kappa(s/2)$.

Hence

$$x(s) = \int_0^s \cos\left(\frac{\kappa}{2s}t^2\right)dt$$
$$y(s) = \int_0^s \sin\left(\frac{\kappa}{2s}t^2\right)dt \quad (17)$$

These integrals are scaled Fresnel integrals and are given by

$$\mathbf{C}(s) = \int_0^s \cos\left(\frac{\kappa}{2s}t^2\right)dt$$
$$\mathbf{S}(s) = \int_0^s \sin\left(\frac{\kappa}{2s}t^2\right)dt \quad (18)$$

Hence

$$x(s) = \mathbf{C}(s)$$
$$y(s) = \mathbf{S}(s) \quad (19)$$

The integrals can be evaluated by a change of variable, given by

$$\bar{t} = \sqrt{\frac{\kappa}{2s}}t$$
$$\bar{s} = \sqrt{\frac{\kappa}{2s}}s = \sqrt{\frac{\kappa s}{2}} \quad (20)$$

Hence

$$dt = \sqrt{\frac{2s}{\kappa}}d\bar{t} \quad (21)$$

and the integrals can be rewritten in the form

$$\mathbf{C}(s) = \sqrt{\frac{2s}{\kappa}}\int_0^{\bar{s}} \cos((\bar{t})^2)\,d\bar{t}$$
$$\mathbf{S}(s) = \sqrt{\frac{2s}{\kappa}}\int_0^{\bar{s}} \sin((\bar{t})^2)\,d\bar{t} \quad (22)$$

Reconstructing this from the radius vector $\mathbf{v}_r$ and the connecting vector $\mathbf{v}_a$ (refer Fig. 5):

$$\mathbf{p} = \mathbf{v}_r + \mathbf{v}_a = \rho\mathbf{t}_r + \alpha\mathbf{t}_a \quad (23)$$

where ρ and α are the lengths of the two vectors. As both $\mathbf{t}_r$ and $\mathbf{t}_a$ are basis vectors, both are of unit length. The unit vectors $\mathbf{t}_r$ and $\mathbf{t}_a$ can be written as

$$\mathbf{t}_r = \begin{pmatrix} 0 \\ 1 \end{pmatrix}$$
$$\mathbf{t}_a = \begin{pmatrix} \sin(\theta) \\ -\cos(\theta) \end{pmatrix} \quad (24)$$

Hence

$$\mathbf{p} = \begin{pmatrix} \mathbf{C}(s) \\ \mathbf{S}(s) \end{pmatrix} = \rho\begin{pmatrix} 0 \\ 1 \end{pmatrix} + \alpha\begin{pmatrix} \sin(\theta) \\ -\cos(\theta) \end{pmatrix} \quad (25)$$

This gives

$$\alpha = \frac{\mathbf{C}(s)}{\sin(\theta)}$$
$$\rho = \left(\mathbf{S}(s) + \frac{1}{\tan(\theta)}\mathbf{C}(s)\right) \quad \text{for } \theta > 0 \quad (26)$$

Now

$$\theta_t = \frac{\kappa}{2}s \quad (27)$$

Converting to angles using $\theta_t = (\kappa/2)s$,

$$\alpha = \frac{\mathbf{C}\left(\frac{2\theta_t}{\kappa}\right)}{\sin(\theta_t)}$$
$$\rho = \left[\mathbf{S}\left(\frac{2\theta_t}{\kappa}\right) + \frac{1}{\tan(\theta_t)}\mathbf{C}\left(\frac{2\theta_t}{\kappa}\right)\right] \quad (28)$$

where

$$\mathbf{C}(\theta_t) = \frac{2}{\kappa}\sqrt{\theta_t}\int_0^{\sqrt{\theta_t}} \cos((\bar{t})^2)\,d\bar{t}$$
$$\mathbf{S}(\theta_t) = \frac{2}{\kappa}\sqrt{\theta_t}\int_0^{\sqrt{\theta_t}} \sin((\bar{t})^2)\,d\bar{t} \quad (29)$$

This implies that there is no closed form solution to the clothoid trajectory. In order to compute a solution, the tangent and normal vectors have to be computed. Thus a clothoid arc can be designed from its curvature profile $\kappa(s)$.

7.3. Dubins path with clothoid arcs

A CLC (circle–line–circle) type Dubins path is shown in Fig. 9. It shows two circles of radius ρ and τ, and ($\mathbf{t}$,$\mathbf{n}$) form a frame with unit tangent and normal vectors. The subscripts s, and f, respectively, denote start and finish and vector $\mathbf{a}_c$ is the connecting vector. The sign of the manoeuvre can be determined by considering the centre line between the two positions. Viewed from each position a positive or negative rotation from the tangent vector to the centre vector $\vec{\mathbf{c}}$ will define the sign of the curvature for each manoeuvre. From the figure

$$\mathbf{r}_i = \mathbf{e}_i\begin{pmatrix} 0 \\ \pm\rho_s \end{pmatrix}$$
$$\mathbf{e}_i = [\mathbf{t}_i \;\; \mathbf{n}_i] \quad (30)$$

where ρ_s is the radius of the initial manoeuvre.

Similarly

$$\mathbf{r}_f = \mathbf{e}_f\begin{pmatrix} 0 \\ \pm\rho_f \end{pmatrix}$$
$$\mathbf{e}_f = [\mathbf{t}_f \;\; \mathbf{n}_f] \quad (31)$$

where ρ_f is the radius of the final manoeuvre.

The Frenet basis vectors are related by

$$\mathbf{e}_f = \mathbf{R}(\theta)\,\mathbf{e}_s \quad (32)$$

where $\mathbf{R}(\theta)$ is the rotation matrix required to change the axis set from start to finish axes.

Hence

$$\mathbf{R}(\theta) = \mathbf{e}_s\mathbf{e}_{f'} \quad (33)$$

The connecting vectors $\mathbf{a}_s$, $\mathbf{a}_f$, and $\mathbf{a}_c$ form an orthogonal set of vectors. In order to determine the vectors, first the connecting vector $\mathbf{a}_c$ is defined in both initial and final axes, as

$$\mathbf{e}_c = \mathbf{R}(\theta_s)\,\mathbf{e}_s$$
$$\mathbf{e}_f = \mathbf{R}(\theta_f)\,\mathbf{e}_c \quad (34)$$

where $\mathbf{e}_c$ is the basis set defining the connecting vector.

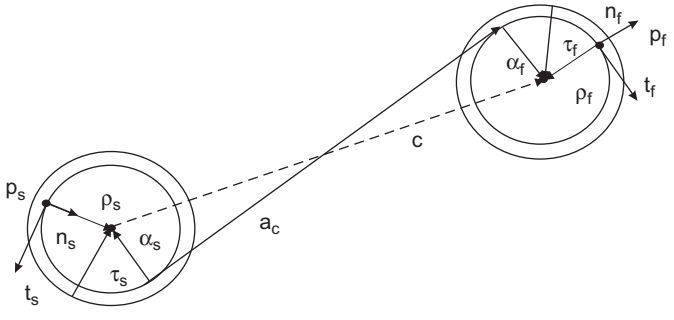

Fig. 9. Dubins path with clothoid arcs in place of circular arcs.

Hence, the total rotation matrix $\mathbf{R}(\theta)$ is given by

$$\mathbf{R}(\theta) = \mathbf{R}(\theta_f)\mathbf{R}(\theta_s) \tag{35}$$

If the position of the final point $\mathbf{p}_f$ relative to the start position $\mathbf{p}_s$ is measured in start axes $\mathbf{e}_s$:

$$\mathbf{p}_f - \mathbf{p}_s = \mathbf{e}_s\mathbf{p}$$
$$\mathbf{p} = \begin{pmatrix} p_t \\ p_n \end{pmatrix} \tag{36}$$

Hence, the vector sum for the position vector in start axes is given by

$$\mathbf{p} = \boldsymbol{\rho}_s - \boldsymbol{\alpha}_s + \mathbf{a}_c + \boldsymbol{\alpha}_f - \boldsymbol{\rho}_f$$
$$\mathbf{p} - \boldsymbol{\rho}_s + \boldsymbol{\rho}_f = -\boldsymbol{\alpha}_s + \mathbf{a}_c + \boldsymbol{\alpha}_f \tag{37}$$

The left hand side of this equation represents the vector connecting the centres of the turn circles. Hence

$$\mathbf{c} = -\boldsymbol{\alpha}_s + \mathbf{a}_c + \boldsymbol{\alpha}_f \tag{38}$$

The centre vector $\mathbf{c}$ can be written in start axes, to give

$$\mathbf{c} = c\mathbf{t}_c = \mathbf{e}_{ct}\begin{pmatrix} c \\ 0 \end{pmatrix}$$
$$\mathbf{e}_{ct} = [\mathbf{t}_c \;\; \mathbf{n}_c] \tag{39}$$

where $\mathbf{e}_{ct}$ is the basis vector set of the centre vector.

The remaining connecting vectors $\boldsymbol{\alpha}_s$, $\boldsymbol{\alpha}_f$, and $\mathbf{a}_c$ can be written in terms of the start basis vectors, as

$$\boldsymbol{\alpha}_s = \mathbf{R}(\theta_s)'\begin{pmatrix} 0 \\ \pm\rho_s \end{pmatrix}$$
$$\boldsymbol{\alpha}_f = \mathbf{R}(\theta_s)'\begin{pmatrix} 0 \\ \pm\rho_f \end{pmatrix}$$
$$\mathbf{a}_c = \mathbf{R}(\theta_s)'\begin{pmatrix} a \\ 0 \end{pmatrix} \tag{40}$$

The centre vector (38), now becomes

$$c\mathbf{t}_{ct} = -\mathbf{R}(\theta_s)'\begin{pmatrix} 0 \\ \pm\rho_s \end{pmatrix} + \mathbf{R}(\theta_s)'\begin{pmatrix} a \\ 0 \end{pmatrix} + \mathbf{R}(\theta_s)'\begin{pmatrix} 0 \\ \pm\rho_f \end{pmatrix}$$
$$= \mathbf{R}(\theta_s)'\begin{pmatrix} a \\ \pm\rho_f - \pm\rho_s \end{pmatrix} \tag{41}$$

Normalising the centre vector to unit magnitude, gives

$$\mathbf{t}_{ct} = \mathbf{R}(\theta_s)'\frac{1}{c}\begin{pmatrix} a \\ \pm\rho_f - \pm\rho_s \end{pmatrix} \tag{42}$$

This is a rotation equation, that represents the rotation of a unit vector. Hence, the right hand vector must have unit magnitude, to give

$$\left|\frac{1}{c}\begin{pmatrix} a \\ \pm\rho_f - \pm\rho_s \end{pmatrix}\right| = 1 \tag{43}$$

or

$$\left(\frac{a}{c}\right)^2 + \frac{1}{c^2}(\pm\rho_f - \pm\rho_s)^2 = 1$$
$$\left(\frac{a}{c}\right)^2 = 1 - \frac{1}{c^2}(\pm\rho_f - \pm\rho_s)^2 \tag{44}$$

This can be used to test for a feasible solution, by

$$1 - \frac{1}{c^2}(\pm\rho_f - \pm\rho_s)^2 > 0 \tag{45}$$

In order to compute the rotation angle θ_s, the equation can be written in the form

$$\mathbf{t}_{ct} = \mathbf{R}(\theta_s)'\frac{1}{c}\begin{pmatrix} \beta \\ \gamma \end{pmatrix}$$
$$\mathbf{R}(\theta_s) = \begin{pmatrix} \cos(\theta_s) & -\sin(\theta_s) \\ \sin(\theta_s) & \cos(\theta_s) \end{pmatrix} \tag{46}$$

where $\beta = \sqrt{c^2 - (\pm\rho_f - \pm\rho_s)^2}$ and $\gamma = (\pm\rho_f - \pm\rho_s)$.

Expanding this and solving for θ_s gives

$$\cos(\theta_s)\frac{\sqrt{c^2 - (\pm\rho_f - \pm\rho_s)^2}}{c} + \sin(\theta_s)\frac{(\pm\rho_f - \pm\rho_s)}{c} = t_{ct1}$$
$$-\sin(\theta_s)\frac{\sqrt{c^2 - (\pm\rho_f - \pm\rho_s)^2}}{c} + \cos(\theta_s)\frac{(\pm\rho_f - \pm\rho_s)}{c} = t_{ct2} \tag{47}$$

or

$$\frac{1}{c}\begin{pmatrix} \sqrt{c^2 - (\pm\rho_f - \pm\rho_s)^2} & (\pm\rho_f - \pm\rho_s) \\ -(\pm\rho_f - \pm\rho_s) & \sqrt{c^2 - (\pm\rho_f - \pm\rho_s)^2} \end{pmatrix}\begin{pmatrix} \cos(\theta_s) \\ \sin(\theta_s) \end{pmatrix} = \mathbf{t}_{ct} \tag{48}$$

Solving for θ_s gives

$$\begin{pmatrix} \cos(\theta_s) \\ \sin(\theta_s) \end{pmatrix} = \frac{1}{c}\begin{pmatrix} \beta & -\gamma \\ \gamma & \beta \end{pmatrix}\mathbf{t}_{ct}$$

Hence

$$\theta_s = \tan^{-1}(\sin(\theta_s), \cos(\theta_s)) \tag{49}$$

The final angle θ_f can then be determined using

$$\theta = \theta_s + \theta_f$$
$$\theta_f = \theta - \theta_s \tag{50}$$

An alternate solution is

$$\mathbf{R}(\theta_s)\mathbf{t}_{ct} = \left(\frac{1}{c}\right)\begin{pmatrix} \beta \\ \gamma \end{pmatrix} \tag{51}$$

Expanding this gives

$$\begin{pmatrix} \cos(\theta_s) \\ \sin(\theta_s) \end{pmatrix} = \frac{1}{\Delta}\begin{pmatrix} t_{ct1} & t_{ct2} \\ -t_{ct2} & t_{ct1} \end{pmatrix}\left(\frac{1}{c}\right)\begin{pmatrix} \beta \\ \gamma \end{pmatrix}$$
$$\Delta = t_{ct1}^2 + t_{ct2}^2 = 1 \tag{52}$$

The related Fresnel integrals are given by

$$\mathbf{C}(s) = \int_0^{s_f} \cos(s^2)\,ds$$
$$\mathbf{S}(s) = \int_0^{s_f} \sin(s^2)\,ds \tag{53}$$

Series expansions are given by

$$\mathbf{C}(s) = \sum_{n=0}^{\infty} \frac{(-1)^n}{(2n+1)!(4n+3)} s^{4n+3}$$
$$\mathbf{S}(s) = \sum_{n=0}^{\infty} \frac{(-1)^n}{(2n)!(4n+1)} s^{4n+1} \tag{54}$$

8. Simulation

Two sets of simulations are carried out. In the first case, path planning of three UAVs in an obstacle-free environment is considered. For the clutter-free environment, the Eq. (5)

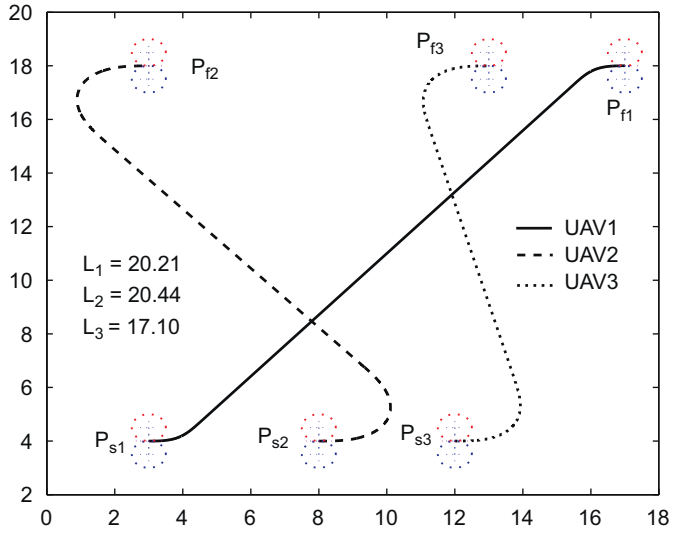

Fig. 10. Initial paths of UAVs.

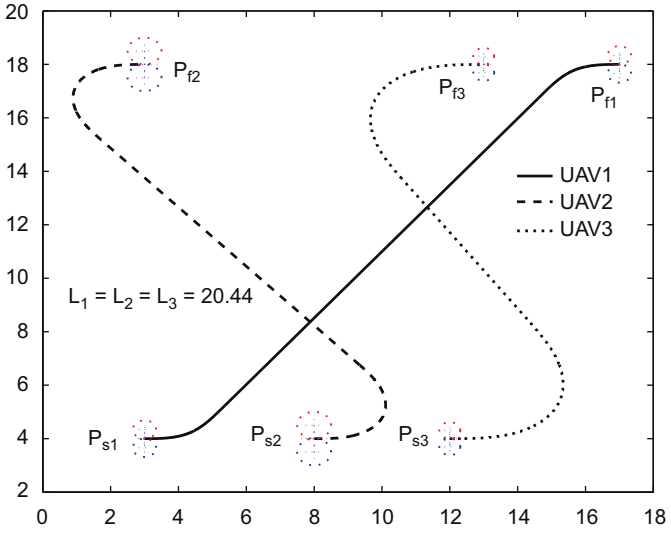

Fig. 11. Flyable paths and equal path-lengths.

changes into

$$P_{s,i,j-1}(x_{s,i,j-1}, y_{s,i,j-1}, \theta_{s,i,j-1}) \xrightarrow{r_{i,j-1}(t)} P_{f,i,j}(x_{f,i,j}, y_{f,i,j}, \theta_{f,i,j})$$
$$i = 1, \ldots, 3, \;\; j = 2, \ldots, n_p, \;\; n_p = 2$$
$$|\kappa_i(t)| < \kappa_{\max}, \coprod_{safe} \coprod_{length} \tag{55}$$

where $\coprod_{safe}$ is limited to inter-collision avoidance of UAVs.

Fig. 10 shows the initial paths of the UAVs: UAV1, UAV2, and UAV3. The initial paths are flyable paths connecting the base and the target which meet the maximum curvature bound. These flyable paths are tested for satisfaction of the safety constraints. From the figure, it can be seen that UAV1 fails to meet the constraint: 'minimum separation distance' as it intersects with the other two paths. The path of UAV1 is tested for the necessary condition (Eq. (7)) and found that the difference in length at the intersection points on the paths of UAV2 and UAV3 is greater than $2R_s$ and hence are safe to fly. The paths of UAV2 and UAV3 are well separated and greater than the safety radius $2R_s$ and hence they meet both the safety constraints. The length of the paths respective are: 20.21, 20.44, and 17.10. The path of UAV2 is thus the reference path. The path lengths of UAV1 and UAV3 are then increased by decreasing the curvature of the clothoid arcs for these UAVs. Fig. 11 shows the resulting paths whose lengths are now equal to (20.44). The safety constraints are tested further on these paths to ensure collision avoidance.

In a cluttered environment, five UAVs each with four way-points are considered. Accordingly, the Eq. (5) becomes

$$P_{s,i,j-1}(x_{s,i,j-1}, y_{s,i,j-1}, \theta_{s,i,j-1}) \xrightarrow{r_{i,j-1}(t)} P_{f,i,j}(x_{f,i,j}, y_{f,i,j}, \theta_{f,i,j})$$
$$i = 1, \ldots, 5, \;\; j = 2, \ldots, n_p, \;\; n_p = 4$$
$$|\kappa_i(t)| < \kappa_{max}, \coprod_{safe} \coprod_{length} \tag{56}$$

Fig. 12 shows the simulation of path planning in a cluttered environment. The poses and threats are generated randomly. The distance between the poses are at least two times greater than the radius of curvature of the UAV. The circles filled with yellow colours are obstacles. Flyable paths are then produced between the poses. From the figure, the paths of the UAVs meet the safety constraints. The threats are handled by generating intermediate way-point/pose as explained in the Section 5.2.3. The intersection of paths with the no-fly zones are determined

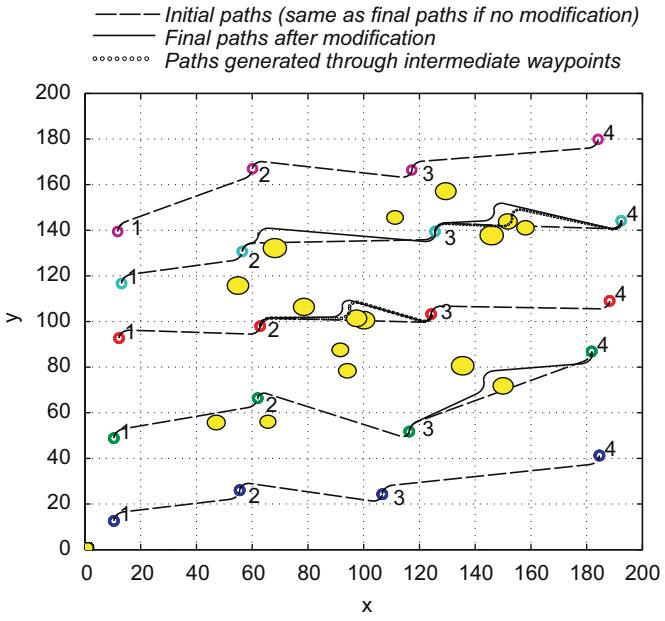

Fig. 12. Five UAVs each with four way-points in cluttered space.

iteratively for the clothoid arc segments, while the intersection of lines with circles is used for the straight line portion of the path. An intermediate pose/way-point is produced for each intersection within the obstacle safety zone. Following this, the paths are re-planned to pass through the new way-points. From the figure, it is also seen that when a path intersects with a single obstacle, re-planning of new path is simple as it only has to avoid a single obstacle. However, re-planning is difficult when obstacles appear in clusters, as in the case of the second and third UAVs. In the case of second UAV, and in between the third and fourth way-points, there are three obstacles in a cluster. The first re-planning of initial path intersects the other obstacle and hence requires further re-planning to avoid all of the obstacles. A similar situation arises for third UAV, where a cluster of two obstacles appear together. Finally, the curvature of the first four paths ordered from the top, are increased to that of the reference path, which is the path length of fifth UAV.

9. Conclusions

This paper describes a new approach to path planning of a group of UAVs using the concept of flyable paths. The proposed approach is simulated with a group of UAVs for simultaneous arrival on target. The flyable path is a Dubins CLC path with clothoid arcs and is designed using the principles of differential geometry. The problem of path planning is formulated by producing feasible paths. The solution is achieved in three phases: (i) producing flyable paths, (ii) meeting the safety constraints, and (iii) producing paths of equal length. The first phase produces flyable paths for the UAVs while the second phase tests the paths for safety constraints and produces safe paths, and the third path produce paths of equal length by increasing the length of the shorter paths to that of a reference path. Thus the path planning problem is reduced to tuning of flyable paths. It is also shown that the 'minimum separation distance' is a sufficient condition and 'non-intersection of paths at equal length' is a necessary condition. Simulations are carried out in a cluttered and clutter-free environments.

References

Bortoff, S. (2000). Path-planning for unmanned air vehicles. In *Proceedings of the American control conference* (pp. 364–368), Chicago, IL.

Chandler, P., Pachter, M., & Rasmussen, S. (2001). UAV cooperative control. In *Proceedings of the American control conference* (Vol. 1, pp. 50–55), Arlington, VA.

Chandler, P., Rasmussen, S., & Pachter, M. (2000). UAV cooperative path planning. In *Proceedings of AIAA guidance, navigation and control conference*, Denver, CO.

Dong, J., & Vagners, J. (2004). Parallel evolutionary algorithms for UAV path planning. In *AIAA first intelligent systems technical conference*, Chicago, IL, 20–22 September.

Dubins, L. (1957). On the curves of minimal length with a constraint on average curvature, and with prescribed initial and terminal positions and tangents. *American Journal of Mathematics*, *79*(3), 497–516.

Eagle, J., & Yee, J. (1990). An optimal branch-and-bound procedure for the constrained path, moving target search problem. *Operations Research*, *28*(1), 110–114.

Judd, K., & McClain, T. (2001). Spline based path planning for unmanned air vehicles. In *Proceedings of the AIAA guidance, navigation and control conference*.

Lipschutz, M. M. (1969). *Schaum's outline of differential geometry*. New York: McGraw-Hill.

Mclain, T. W., & Beard, R. W. (2000). Trajectory planning for coordinated rendezvous of Unmanned Air Vehicles. In *Proceedings of the AIAA guidance, navigation and control conference* (Vol. AIAA-2000-4369:AAO-37126), Denver, CO.

Nikolos, I., Valavanis, K., Tsourveloudis, N., & Kostaras, A. (2003). Evolutionary algorithm based offline/online path planner for UAV navigation. *IEEE Transactions on Systems, Man, and Cybernetics—Part B*, *33*, 898–912.

Rabbath, C., Gagnon, E., & Lauzon, M. (2004). On the cooperative control of multiple unmanned aerial vehicles. *IEEE Canadian Review*, 8–15.

Scheuer, A., & Fraichard, T. (1997). Collision-free continuous curvature path planning for car-like robots. In *IEEE international conference on robotics and automation* (pp. 867–873), Albuquerque, NM.

Schouwenaars, T., Feron, E., & How, J. (2006). Multi-vehicle path planning for non-line of sight communication. In *Proceedings of the American control conference*, MN, USA, June 14–16.

Segovia, S., Rombaut, M., Preciado, A., & Meizel, D. (1991). Comparative study of the different methods of path generation for a mobile robot in a free environment. In *Proceedings of the international conference on advanced robotics* (pp. 1667–1670).

Shanmugavel, M., Tsourdos, A., Żbikowski, R., & White, B. A. (2005). Path planning of multiple UAVs using Dubins sets . In *Proceedings of the AIAA guidance, navigation and control conference and exhibition* (Vol. AIAA-2005-5827), San Francisco, CA, August 15–18.

Shanmugavel, M., Tsourdos, A., Żbikowski, R., & White, B. A. (2006). 3D Dubins sets based coordinated path planning for swarm of UAVs. In *Proceedings of the* AIAA *guidance, navigation, and control conference and exhibition*, (Vol. AIAA-2006-6211), Keystone, CO, August 21–24.

Shanmugavel, M., Tsourdos, A., Żbikowski, R., White, B. A., Rabbath, C. A., & Lechevin, N. (2006). A solution to simultaneous arrival of multiple UAVs using Pythagorean hodograph curves. In *Proceedings of the American control conference*, Minneapolis, MN, USA, June 14–16.

Shima, T., Rasmussen, S., & Sparks, A. (2005). UAV cooperative multiple task assignments using genetic algorithms. In *Proceedings of the American control conference*, Oregon.

Uny Cao, Y., Fukunaga, A., & Kahng, A. (1997). Cooperative mobile robotics: Antecedents and directions. *Autonomous Robots*, *4*, 7–27.

Wilson, J. (2007). UAV worldwide roundup 2007. *Aerospace America*, *5*, 30–37.

Zabarankin, M., Uryasev, S., & Pardalos, P. (2001). Optimal risk path algorithms. In R. Murphey & P. Pardaolas (Eds.), *Cooperative control and optimization* (pp. 271–303). Dordrecht: Kluwer Academic Publishers.

Zhang, D., Wang, L., & Yu, J. (2008). Geometric topology based cooperation for multiple robots in adversarial environments. *Control Engineering Practice*, *16*, 1092–1100.

Zheng, C., Li, L., Xu, F., Sun, F., & Ding, M. (2005). Evolutionary route planner for unmanned air vehicles. *IEEE Transactions on Robotics*, *21*(4), 609–620.